AN “OFF-THE-SHELF” POST FIRE HYDROLOGIC MODEL FOR CALIFORNIA WILDFIRES

A Thesis

Presented to

The Faculty of the Department of Civil Engineering

California State University, Los Angeles

In Partial Fulfillment

of the Requirements for the Degree

Master of Science

in

Civil Engineering

By

Adolfo A Retana-Garcia

May 2024

See "Sample Pages" for Thesis on the Grad Studies website for additional information about filling in this template. Replace, add, or delete information as needed. To indent from the left in Table of Contents, use Tab key. Remove this note by double-clicking in this section and deleting.

© 2024

Adolfo A Retana-Garcia

ALL RIGHTS RESERVED

See "Sample Pages" for Thesis on the Grad Studies website for additional information about filling in this template. Replace, add, or delete information as needed. To indent from the left in Table of Contents, use Tab key. Remove this note by double-clicking in this section and deleting.

The thesis of Adolfo A Retana-Garcia is approved.

Sonya R. Lopez, Committee Chair

Jingjing Li

Welson Kwan

Gustavo Menezes, Department Chair

California State University, Los Angeles

May 2024

See "Sample Pages" for Thesis on the Grad Studies website for additional information about filling in this template. Replace, add, or delete information as needed. To indent from the left in Table of Contents, use Tab key. Remove this note by double-clicking in this section and deleting.

ABSTRACT

AN "OFF-THE-SHELF" POST FIRE HYDROLOGIC MODEL FOR CALIFORNIA WILDFIRES

By

Adolfo A Retana-Garcia

Frequent wildfires have become a significant disruptor of forest ecosystems, driven by climate change, land use alterations, and human activities. While wildfires play a crucial role in natural processes, their increasing frequency necessitates a deeper understanding of their ecological, social, and economic impacts. This study delves into the intricacies of wildfire dynamics by using a hydrological model called ParFlow-CLM that requires calibrating and validating datasets to analyze water resources, soil conditions, burn ratios, and other vital parameters. This research delves into three major wildfires of significant impact: the August, Delta, and Creek fires. Starting with the August fire, an extensive wildfire ravaged the Coast Range of Northern California from August 16, 2020, to November 15, 2020. Following this, the Delta Fire, a notable 2018 wildfire in the Shasta-Trinity National Forest, unfolded from September 5, 2018, to October 07, 2018. Lastly, the Creek Fire occurred in central California's Sierra National Forest, spanning Fresno and Madera counties from September 4, 2020, to December 24, 2020.

We are directing our attention towards examining the enduring consequences stemming from the fires, which encompass the formation of a hydrophobic layer, loss of vegetation, alterations in soil composition, and modifications in both surface and subsurface flow dynamics. This includes investigating water flux, long-term storage in the subsurface, and the potential for floods and hazardous overland flow. By developing an 'off-the-shelf'

See "Sample Pages" for Thesis on the Grad Studies website for additional information about filling in this template. Replace, add, or delete information as needed. To indent from the left in Table of Contents, use Tab key. Remove this note by double-clicking in this section and deleting.

model, we lay the groundwork for a versatile tool applicable to diverse research needs. Our study compared ECOSTRESS and MODIS data, with ECOSTRESS offering limited insights into ET accuracy. Despite data constraints, our model showed a moderate correlation (R = 0.4416) with ECOSTRESS and a weaker correlation (R = 0.3747) with MODIS but benefited from a more extensive data set. The project's limitations included restricted ECOSTRESS data and challenges in configuring the model for fire conditions but valuable insights for future study improvement.

ACKNOWLEDGMENTS

I would like to express my heartfelt gratitude to my mother, Francisca Garcia, for her endless sacrifices and unwavering encouragement to pursue my dreams. Despite the difficult times, she always brought a smile to my face and motivated me to push my limits.

Additionally, I extend my deepest gratitude to my advisor, Dr. Sonya R. Lopez, for her invaluable mental, scholarly, and emotional support throughout the years. Her guidance during the long nights and hard work helped me produce a thesis that I am incredibly proud of.

See "Sample Pages" for Thesis on the Grad Studies website for additional information about filling in this template. Replace, add, or delete information as needed. To indent from the left in Table of Contents, use Tab key. Remove this note by double-clicking in this section and deleting.

TABLE OF CONTENTS

ABSTRACT ..... *iv*

ACKNOWLEDGMENTS ..... *v*

LIST OF FIGURES ..... *vii*

CHAPTER 1 ..... *1*

INTRODUCTION *1*

CHAPTER 2 ..... *5*

MATERIALS AND METHODS *5*

Study Site **5**

ParFlow-CLM **7**

Model Configuration **10**

Model Domain **16**

Model Validation **18**

CHAPTER 3 ..... *20*

RESULTS *20*

Issues with Model Simulations **20**

Observed vs Simulated **21**

Data Limitations and Issues **25**

CHAPTER 4 ..... *26*

CONCLUSION *26*

REFERENCES *28*

See "Sample Pages" for Thesis on the Grad Studies website for additional information about filling in this template. Replace, add, or delete information as needed. To indent from the left in Table of Contents, use Tab key. Remove this note by double-clicking in this section and deleting.

LIST OF TABLES

Table 1 - Description of the seventeen parameters used to estimate ET; each parameter changes for each land use classification 9
Table 2 - Description of the original 18 Landcover Types and 14 new medium burn classifications (32 total) that define vegetation parameters. 11-12
Table 3 - Satellite observations required for domain development (NLDAS-2, BAER, DEM) and model comparison (MODIS and ECOSTRESS)..... 13
Table 4 - Variable discretization in the z-direction for the total depth (nx*dz = 884(Delta) and 1692(Creek))..... 17-18

LIST OF FIGURES

Figure 1- The Delta Fire in 2018 Consisted of the Slate Creek-Sacramento River, East Fork, Trinity River Watersheds 6
Figure 2 - The Creek Fire in 2020 Consisted of Chiquito Creek, Stevenson Creek-San Joaquin River Watersheds..... 7
Figure 3 - Representation of ParFlow 8
Figure 4 - Required CLM.F90 update to ParFlow-CLM..... 11
Figure 5 - Workflow 15
Figure 6 - Raw ECOSTRESSV Data from 09/05/1/2018- 04/01/2019 Vs Pre/Post Fires Data for Slate Creek-Sacramento River, East Fork 21
Figure 7 - Moving Mean ECOSTRESSV Data from 09/05/1/2018- 04/01/2019 Vs Pre/Post Fires Data for Slate Creek-Sacramento River, East Fork 22
Figure 8 - ECOSTRESS Vs. Simulated ET Correlation 23
Figure 9 - MODIS Data from 09/05/1/2016- 04/01/2019 Vs Pre/Post Fires Data for Slate Creek-Sacramento River, East Fork..... 24
Figure 10 - MODIS Vs. Simulated ET Correlation 25

CHAPTER 1

INTRODUCTION

Wildfires, although often associated with destruction, are a natural phenomenon that plays a pivotal role in shaping our landscapes and ecosystems (Stevens-Rumann, Morgan, 2019) (Zavala, Celis, Jordan, 2014) (Pérez-Cabello, Montorio, Borini Alves, 2021) (Hernández Ayala, Mann, Grosvenor, 2021). These events are unpredictable and vary in magnitude; wildfires have a remarkable impact on society, ecosystems, hydrological parameters, and the broader environment, making them a complex and dynamic force of nature that demands ongoing research. (Stevens-Rumann, Morgan, 2019) (Hernández Ayala, Mann, Grosvenor, 2021) (Jung, Hogue, Rademacher, Meixner, 2008) The frequency and burn severity of these natural disasters significantly varies depending on geographic location, climate, and existing hydrological conditions such as soil moisture and land cover type. (Jensen, Reager, Zajic, Rousseau, Rodell, Hinkley, 2018) (Ilan Stavi, 2019). In the past four decades, the Southwestern regions of the United States have witnessed a significant increase in wildfires (Miller, Safford, 2012). These areas often go through a recovery cycle, only to see a resurgence of wildfires in the same geographic location (Miller, Safford, 2012). Studies suggest that regions with low soil moisture levels are at a higher risk of experiencing more frequent and more extensive wildfires (Buhk, Meyn, Jentsch, 2006) (Schnur, Xie, Wang, 2010) (Jensen, Reager, Zajic, Rousseau, Rodell, Hinkley, 2017) (Hernández Ayala, Mann, Grosvenor, 2021). Jensen et al. (2017) demonstrated that areas characterized as arid desert or dry environments, similar to our study sites in California, experience low soil moisture levels and face an elevated risk of wildfires. Similarly, Buhk et al. (2006) highlighted the vulnerability of regions with

depleted soil moisture through the fire season (Summer), expressing concerns of fire resurgences. Hernández Ayala et al. (2021) further indicated that California is known for low soil moisture levels and is predisposed to more frequent and extensive wildfires because of high temperature seasons. Together, these studies provide compelling evidence that areas with similar climate to California are at a heightened risk of experiencing wildfires of greater frequency and magnitude. Researchers predict that the frequency and intensity of wildfires will continue to rise over the next century due to the impacts of climate change (A.L. Westerling, B.P Bryant, 2007) (Mathew W. Jones, Adam Smith, Richard Betts, Josep G. Candadell, I. Colin Prentice, Corinne Le Quere, 2020) (Marcos Rodrigues, Paloma Ibarra, Maite Echeverria 2014). Southern California is a perfect example of this trend, as it commonly experiences these occurrences due to its high exposure to heat and drought seasons that lead to dry vegetation. (Stevens-Rumann, Morgan, 2019) (Hernández Ayala, Mann, Grosvenor, 2021) (Jung, Hogue, Rademacher, Meixner, 2008). Under these conditions, it is typical for "Megafires" to develop and pose a higher threat as they have a more significant impact, leading to post-fire erosion, water supply impacts, and destructive flash flooding or debris flow. Megafires are highly intensive wildfires that cover a vast area of vegetation and have an extremely high burn intensity capable of changing soil characteristics and immensely affecting the hydrologic response of watersheds. (Moody, Ebel, 2012) (Neary, Gottfried, DeBano, Tecle, 2003) (Nawa Raj Pradhan, Ian Floyd, 2021) (Alicia M. Kinoshita, Terri S. Hogue, 2011) (Van Leeuwen, 2008). Low-severity fires have a minimal impact on aboveground vegetation, leaving most of it unharmed. On the other hand, high-severity fires (Megafires) cause extensive damage, often killing all aboveground vegetation resulting in a significant

reduction in the leaf area available for transpiration. The effects of high-severity fires can last for decades as the vegetation slowly recovers from the intense burning. (M. Poulos, Barton, W. Koch, E. Kolb, E. Thode, 2021)

Assessing burn severity following a wildfire is crucial for understanding changes in soil and overland flow dynamics. When a wildfire occurs, the organic compounds in the soil vaporize, reducing the adhesion between soil particles and resulting in the formation of a hydrophobic layer (Ilan Stavi, 2019) (Stavi, Barkai, Knoll, Glion, Katra, Brook, Zaady, 2016) (Clothiera, Vogelera, and Magesan, 1999). This hydrophobic layer transforms the very nature of the soil, turning it into an impermeable barrier that repels water. This leads to an increase in overland flow, reduced water infiltration into the subsurface, and, in most instances, inhibited vegetation growth, leading to a decrease in evapotranspiration for several years during post-fire recovery. (B.E Clothier, I. Vogeler, G.N Magesan, 2000) (L.F. Debano, 2000). (Ilan Stavi, 2019) (Jane G Cawson, Petter Nyman Hugh G. Smith, Patrick N.J. Lane, Gary J. Sheridan, 2016)

Over the years, numerous studies have illustrated the effectiveness of remote sensing in assessing wildfire impacts. (Van Leeuwen, 2008) (Stisen, Jensen, Sandholt, Grimes, 2008) (Kittel, Nielsen, Tøttrup, Bauer-Gottwein, 2018). Satellite-based remote sensing technologies have revolutionized wildfire research and have become valuable tools for monitoring and evaluating post-fire conditions. Satellite observations can be used to meet the significant high-resolution data demands of hydrologic models needed to define the domain and calibrate model outputs effectively. (Stisen, Jensen, Sandholt, Grimes, 2008) (Kittel, Nielsen, Tøttrup, Bauer-Gottwein, 2018). Standard remote sensing datasets used for model parameterization include the Land Remote-Sensing Satellite System

(LANDSAT), Advanced Very High-Resolution Radiometer (AVHRR), Moderate Resolution Imaging Spectroradiometer (MODIS), and Ecosystem Spaceborne Thermal Radiometer Experiment on Space Station (ECOSTRESS). Researchers methods consist of using techniques and satellite measurements such as Multispectral Scanner (MSS), Thematic Mapper (TM), Enhanced Thematic Mapper Plus (ETM+), Normalized Difference Vegetation Index (NDVI), Enhanced Vegetation Index (EVI), and Advanced Land Imager (ALI) to quantify and categorize vegetation (Viana Soto, Aguado, Martinez, 2017) (Perez-Cabello, Montorio, Alves, 2021) (Van Leeuwen, 2008).

Post-fire analysis has become extremely popular, but there are still several gaps in this research topic. Studies must address the long-term ecological impact of wildfires on diverse ecosystems and improve post-fire recovery and resilience strategies. It is crucial to consider the deformation of the hydrophobic layer in the hydrologic model for up to 1-10 years or more; no hydrologic models attempt to demonstrate this process. This project aims to create a user-friendly, off-the-shelf modeling framework that is readily accessible even to researchers and land managers lacking prior modeling expertise and coding. We aim to develop a postfire hydrologic modeling framework that bridges the knowledge gaps surrounding wildfires' impacts on our ecological, social, and economic platforms. We seek to explicitly account for the formation of hydrophobic layers and explore its deformation. In addition, we would like to demonstrate the effectiveness of utilizing open-access satellite observations to enrich our model's calibration. Our team has developed pre-processing scripts for land use, elevation, burn maps, and evapotranspiration satellite products from NASA, NASA JPL, the US Forest Service, and the US Geological Survey to execute ParFlow-CLM watershed models that represent pre- and post-wildfire hydrologic

conditions. The framework of our study allows for individual control and spatial variation of hydraulic properties, making it a well-suited tool for investigating post-wildfire hydrology in landscapes.

CHAPTER 2

MATERIALS AND METHODS

Study Site

We identified three significant wildfires, Delta Fire (2018), Creek Fire (2020), and August Fire (2020), as the primary focus for our study. Although these fires are all located in California, they vary in size and burn severity, antecedent moisture conditions, and vegetation type. The Delta Fire was part of a series of wildfires that ravaged the Shasta-Trinity National Forest in the northern part of California. The fire ignited on September 05, 2018, by human-related activities still under investigation. The fire burned approximately 63,000 acres with a medium to high burn severity. The burn scar of this fire spanned from 41.08° N, -122.32°E to 40.92° N, -122.60° E. Our model domain consisted of a 30m spatial resolution in the x-y extents and a 15m spatial resolution in the z-direction. The number of cells in the x, y, and z directions were 884, 503, and 15 or over 6 million computation cells.

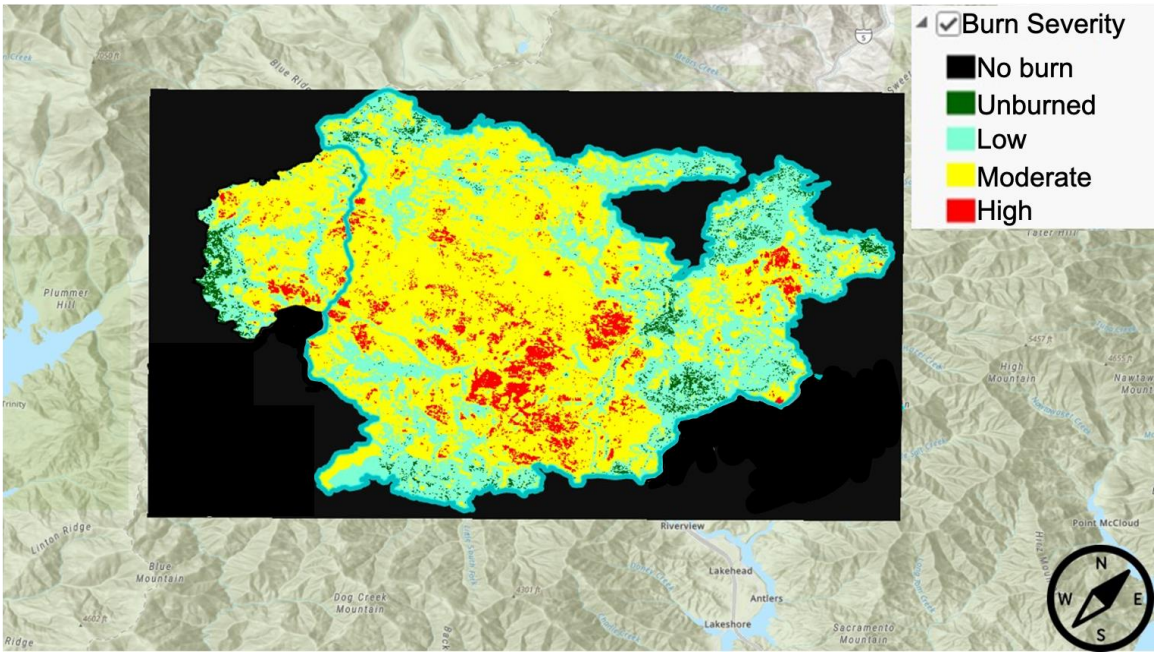


Figure 1: The Delta Fire in 2018 Consisted of the Slate Creek-Sacramento River, East Fork, Trinity River Watersheds

The Creek Fire was a devastating wildfire in the Sierra National Forest in California. The fire ignited on September 4, 2020, by lightning strikes and quickly grew into one of the largest and most destructive wildfires in California's history. The fire was fueled by dry vegetation, hot temperatures, and fierce winds, leading to rapid and unpredictable spread. The fire burned approximately 380,000 acres with a medium to high burn severity ratio. The burn scar of this fire spanned from 37.64° N, -118.94°E to 36.98° N, -119.48° E. The cell dimensions for the model were 30m x 30m x 15m in the x, y, and z. The number of cells in the x, y, and z directions were 1692, 2046, and 15 or almost 52 million computation cells.

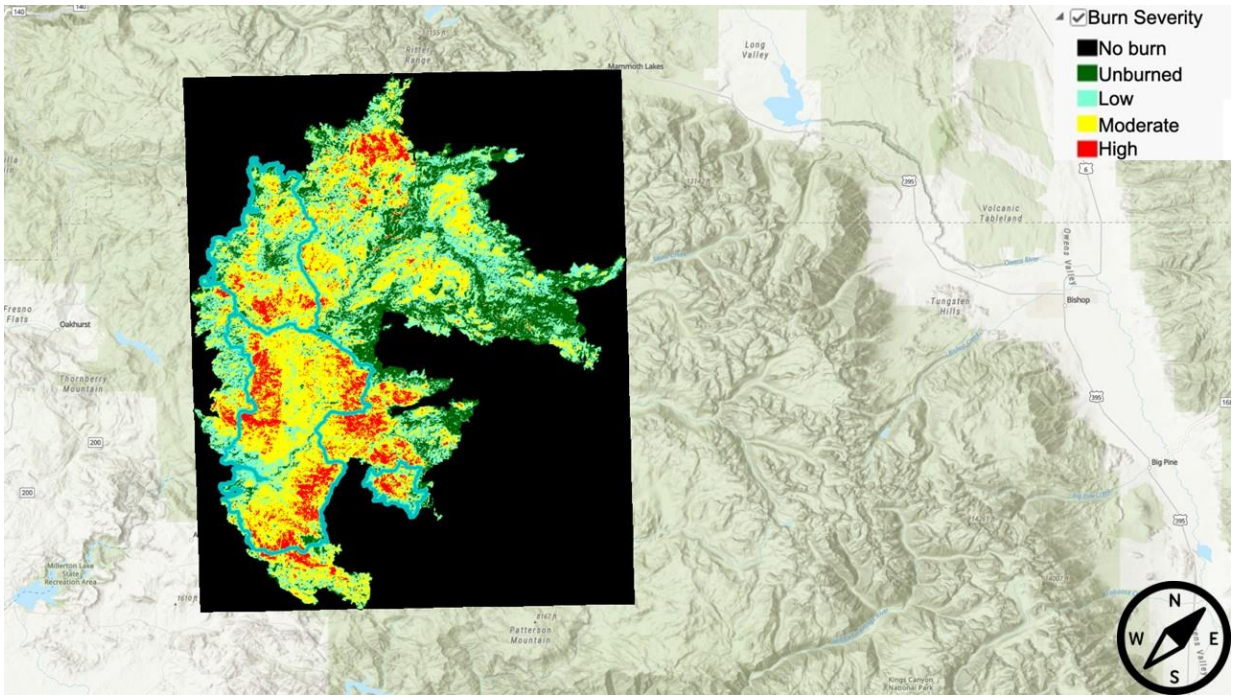


Figure 2: The Creek Fire in 2020 Consisted of Chiquito Creek, Stevenson Creek-San Joaquin River Watersheds.

ParFlow-CLM

We used ParFlow-CLM, a coupled model framework that simulates the surface-subsurface interactions and atmospheric fluxes to simulate our pre- and post-fire hydrologic conditions. (Kollet, Maxwell, 2005). ParFlow is a numerical model that simulates spatially distributed surface and subsurface water flow to demonstrate the hydrological cycle. It combines the three-dimensional groundwater flow, overland flow, and land surface processes using complex equations that help simulate water and energy fluxes in complex real-world domains. ParFlow utilizes and solves an upper boundary condition (Neumann type) combined with the shallow water equations, boundary source-sink, mixed forms of Richard's Equation, and flux relationships from Darcy and Manning's equations.

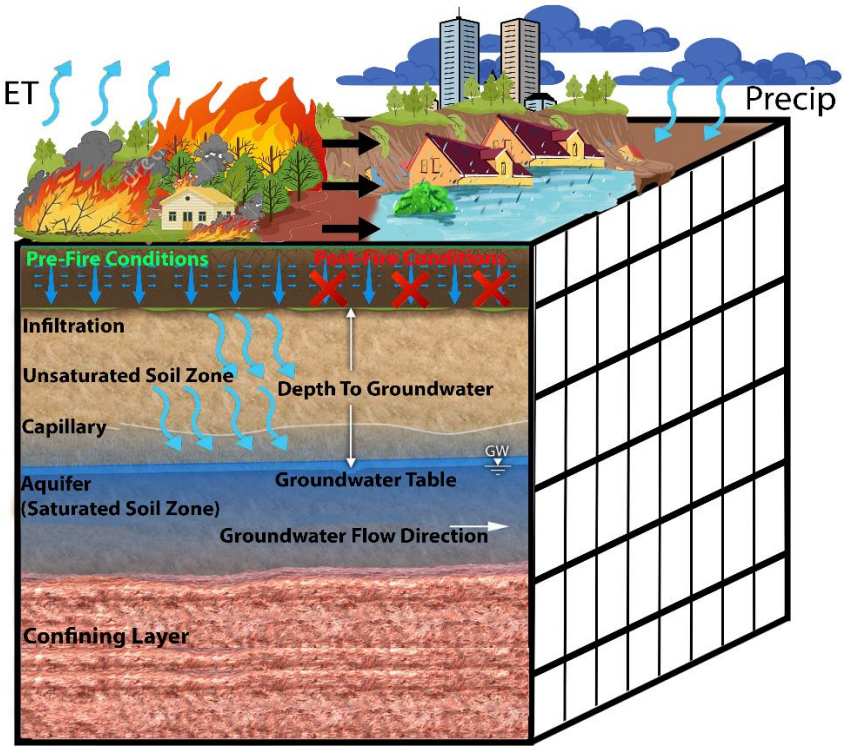


Figure 3: Representation of ParFlow

Mixed Form of Richards' (solving for h): (Kollet, Maxwell, 2005)

$$S_s S_w(h)\frac{\partial h}{\partial t} + \theta\frac{\partial S_w(h)}{\partial t} = \nabla q + q_r(x,z) \qquad \text{Eq 1}$$

Upper Boundary Condition (Neumann type) combined with the Shallow water equation. (solving for the same h): (Kollet, Maxwell, 2005)

$$k(-K_s(x)k_r(h)\nabla(h+z) = \frac{\partial||h,0||}{\partial t} - \nabla\big||h,0|\big|v_{sw} + q_r(x) \qquad \text{Eq 2}$$

Boundary Source-Sink generated from the weather and land surface processes: (Kollet, Maxwell, 2005)

$$q_r(x) = P(x) - E(x) \qquad q_r(x,z) = -E_T(x,z) \qquad \text{Eq 3}$$

Flux Relationships from Darcy and Manning's Equation: (Kollet, Maxwell, 2005)

$$\boldsymbol{q} = K_s(x)k_r(h)[\nabla(h+z)cos\beta_x + sin\beta_x]$$

$$v_x = \frac{\sqrt{S_{f,x}}}{n}\psi_s^{2/3}$$

Eq 4

It is important to note that Richard's Equation and the shallow water equation are two nonlinear equations that demonstrate the interaction between the systems. Solving these equations generates a three-dimensional variably flow using either an orthogonal or terrain-following grid (Maxwell, 2013). ParFlow is coupled with the Community Land Model (CLM), a land surface and atmospheric model that simulates the exchange of energy, water, and momentum between the land surface and the atmosphere. CLM uses the International Geosphere-Biosphere Programme (IGBP) classifications to define *eighteen* types of biomes needed for ParFlow. Each biome type is associated with nineteen physical parameters, including minimum and maximum leaf area index values, aerodynamic resistance, and other essential classifications.

Table 1: Description of the seventeen parameters used to estimate ET; each parameter changes for each land use classification.

#	Variable	Description
1	lai	Maximum leaf area index [-]
2	lai0	Minimum leaf area index [-]
3	sai	Stem area index [-]
4	z0m	Aerodynamic roughness length [m]
5	displa	Displacement height [m]
6	dleaf	Leaf dimension [m]
7	roota	Fitted numerical index of rooting distribution
8	rootb	Fitted numerical index of rooting distribution
9	rhol_vis	leaf reflectance visual spectrum
10	rhol_nir	leaf reflectance near infrared spectrum
11	rhos_vis	stem reflectance visual spectrum
12	rhos_nir	stem reflectance near infrared spectrum
13	taul_vis	leaf transmittance visual spectrum
14	taul_nir	leaf transmittance near infrared spectrum
15	taus_vis	stem transmittance visual spectrum
16	taus_nir	stem transmittance near infrared spectrum
17	xl	leaf/stem orientation index

These parameters play a crucial role in calculating surface evaporation, evapotranspiration from the root zone, conditions related to open canopy, and the overall evapotranspiration within a specified geographical region. The model configuration is defined by grid cells in the x, y, and z directions. The more grid cells we generate, the finer the resolution we receive for our study area. This also means that it comes at a higher computational cost. Every cell within the domain is attributed to specific physical properties, such as saturated hydraulic conductivity, porosity, Leaf Area Index, and Burn Severity, which are instrumental in quantifying changes in hydrological conditions as time progresses.

Model Configuration

ParFlow typically lacks provisions for incorporating burn conditions within its default settings. Our research requires adjustments to these specific files in response to this limitation. In this study, we update the drv_vegp and drv_vegm DAT files utilized by ParFlow-CLM. The default drv_vegp.dat file includes basic parameters that correlate with eighteen specific vegetation types (Table 2), and it is responsible for informing ParFlow-CLM of all the parameters listed on Table 1. The drv_vegm DAT file designates a binary yes or no for each cell in the domain for each landuse type. To consider burned conditions, we manually add fourteen additional vegetation types that now consider medium to high burn. Under medium conditions, the maximum and minimum leaf area index (LAI) are assumed to be 30% of the original parameter value. Under high conditions, the maximum and minimum leaf area index are assumed to be zero for bare soil as there is no vegetation available.

```
!=== Specify grid size using values passed from PF
drv%dx = pdx
drv%dy = pdy
drv%dz = pdz
drv%nc = nx
drv%nr = ny
drv%nt = 32                  ! 18 IGBP land cover classes
drv%ts = dt*3600.d0          ! Assume PF in hours, CLM in seconds
j_incr = nx_f
k_incr = nx_f*ny_f
```

Figure 4: Required CLM.F90 update to ParFlow-CLM

To consider these new medium burn severity classifications, we had to update the default number of landcover classifications in ParFlow-CLM from 18 to 32. We recompiled ParFlow-CLM on the Curie cluster managed by the College of ECST and College of NSS after updating the drv%nt parameter from 18 to 32. Figure 4 highlights the line of code from the CLM.F90 file users must update to include the additional vegetation types that consider medium burn (MED BURN) classifications (summarized in Table 2). The landuse type is defined based on the burn severity map developed by the Burned Area Emergency Response (BAER). All unburned locations did not receive a change in landcover type (Category 1 – 18), any moderate burn severity locations were changed to the medium burn classification of the original landcover type at that location (Category 19 – 32), and landcover type at high burn severity locations were changed to a bare soil classification (Category 18).

Table 2: Description of the original 18 Landcover Types and 14 new medium burn classifications (32 total) that define vegetation parameters.

Original Landcover Types			
Category	**Landcover Types**	**Category**	**Landcover Types**
1	Evergreen needleleaf forests	10	grasslands
2	Evergreen broadleaf forests	11	permanent wetlands
3	Deciduous needleleaf forests	12	croplands
4	deciduous broadleaf forests	13	urban and built-up lands
5	mixed forests	14	cropland / natural vegetation mosaics
6	closed shrublands	15	snow and ice

7	open shrublands	16	barren or sparsely vegetated
8	woody savannas	17	water bodies
9	savannas	18	bare soil
Additional Burn Landcover Types			
19	evergreen needleleaf forests MED BURN	26	woody savannas MED BURN
20	evergreen broadleaf forests MED BURN	27	savannas MED BURN
21	deciduous needleleaf forests MED BURN	28	grasslands MED BURN
22	deciduous broadleaf forests MED BURN	29	permanent wetlands MED BURN
23	mixed forests MED BURN	30	croplands MED BURN
24	closed shrublands MED BURN	31	cropland / natural vegetation mosaics MED BURN
25	open shrublands MED BURN	32	barren or sparsely vegetated MED BURN

This meticulous customization enables us to simulate realistic scenarios based on the burn scar itself, providing a more comprehensive and accurate representation of the complex interactions between vegetation, soil, and water dynamics within the ParFlow framework. The domain matrix is manually customized to represent a range of landscapes, from hillside terrain to entire watersheds. (Condon and Maxwell, 2015); however, the size and precision of the domain are constrained by the available number of processors and computing time. Higher resolution and a more extensive spatial domain demand more computational cells, consequently necessitating more computations per time step.

To produce ParFlow-CLM run files that model post and pre-fire simulations, we developed a pre-processing script in MATLAB. Before running any MATLAB script, the research team synthesized, edited, and formatted raw input files, outlined below using ArcGIS Pro (ESRI, 2011).

Table 3: Satellite observations required for domain development (NLDAS-2, BAER, DEM) and model comparison (MODIS and ECOSTRESS)

Name	Agency Source	Resolution	What it provides
NLDAS-2 (North American Land Data Assimilation System-Version 2)	NASA, NOAA, USDA, Princeton University	Varies (e.g., 1/8th or 1/16th degree)	Land surface model outputs, meteorological data, etc.
BAER (Burned Area Emergency Response)	USGS	Not applicable (program, not dataset)	Emergency response assessments and stabilization data
DEM (Digital Elevation Model)	USGS	Varies (e.g., 1 meter, 30 meters), domain specific	Elevation data for terrain modeling and analysis
MODIS	NASA, USGS	Varies (e.g., 250 meter, 500 meters), domain specific	Remote sensing data for land cover, vegetation, etc.
ECOSTRESS	NASA, JPL	Varies (e.g., 70 meters)	Thermal infrared data for monitoring plant parameters

The North American Land Data Assimilation System-Version 2 (NLDAS-2) dataset encompasses crucial atmospheric variables including air temperature [K], precipitation [mms^{-1}], specific humidity [$kgkg^{-1}$], surface pressure [Pa], incoming shortwave [Wm^{-2}] and longwave radiation [Wm^{-2}], and wind speed [ms^{-1}]. These elements are essential for comprehensively understanding the complex interactions between the atmosphere and land surface processes. NLDAS-2 employs advanced data assimilation techniques, integrating observational data from diverse sources such as weather stations, remote sensing technologies, and satellite observations. This integration ensures the production of high-quality data products that are invaluable for various applications in environmental research, hydrology, and meteorology.

Burned Area Emergency Response (BAER) is a critical post-wildfire assessment process designed to evaluate and mitigate immediate risks to human life, property, and natural resources in the aftermath of a wildfire. (US Forest Service, USDA, 2024) BAER can conduct rapid assessments to identify potential post-fire hazards such as soil erosion, water quality degradation, debris flows, and other environmental concerns. These assessments are essential for guiding emergency response efforts and informing post-fire rehabilitation strategies. BAER utilizes a multidisciplinary approach, drawing on expertise from various fields, including hydrology, soil science, geomorphology, ecology, and forestry. By swiftly assessing the impacts of wildfires and implementing targeted mitigation measures, BAER plays a crucial role in safeguarding ecosystems and communities in fire-affected areas. To further assists our project analysis, we obtained burn severity maps for California covering the years 2016 to 2022 from the United States Geological Survey (USGS) Burned Area Rapid Response (BAER) website (USGS, 2020). These maps vividly depict the extent and severity of fire damage within each affected area or burn scar (Figures 1 and 2). Through this resource, we accessed raw dNBR values, subsequently translating them into saturated hydraulic conductivity (Ksat) using Equation 5. (Atchley, A. L., Kinoshita, A. M., Lopez, S. R., Trader, L., & Middleton, R.,2018)

$$\text{Ksat} = 0.39 * \exp(-0.0056\ \text{dNBR}) \qquad \text{Eq 5}$$

The ECOSTRESS (Ecosystem Spaceborne Thermal Radiometer Experiment on Space Station) mission is pivotal in wildfire research, offering unparalleled insights into post-fire ecosystem dynamics and hydrological processes. (Jet Propulsion Laboratory, NASA, 2024) Developed by NASA, ECOSTRESS provides crucial data for our study sites on land surface temperature, evapotranspiration rates, and vegetation health, all of which are

instrumental in assessing the impacts of wildfires on landscapes. (Joshua B. Fisher, et al. 2020) (K. Meerdink, J. Hook, A. Roberts, A. Abbott, 2019)((Jet Propulsion Laboratory, NASA, 2024) By monitoring thermal emissions from vegetation and soil, ECOSTRESS enables researchers to rapidly detect post-fire changes in ecosystem health, identify areas at risk of vegetation stress or mortality, and evaluate the resilience of ecosystems to fire disturbances. This comprehensive understanding of post-fire dynamics is essential for guiding post-fire management strategies, including rehabilitation efforts to restore ecosystem functionality and mitigate potential hazards such as soil erosion and water quality degradation. Through its precise measurements and global coverage, ECOSTRESS is pivotal in advancing our knowledge of wildfire impacts and supporting informed decision-making for ecosystem resilience and community safety in fire-prone regions.

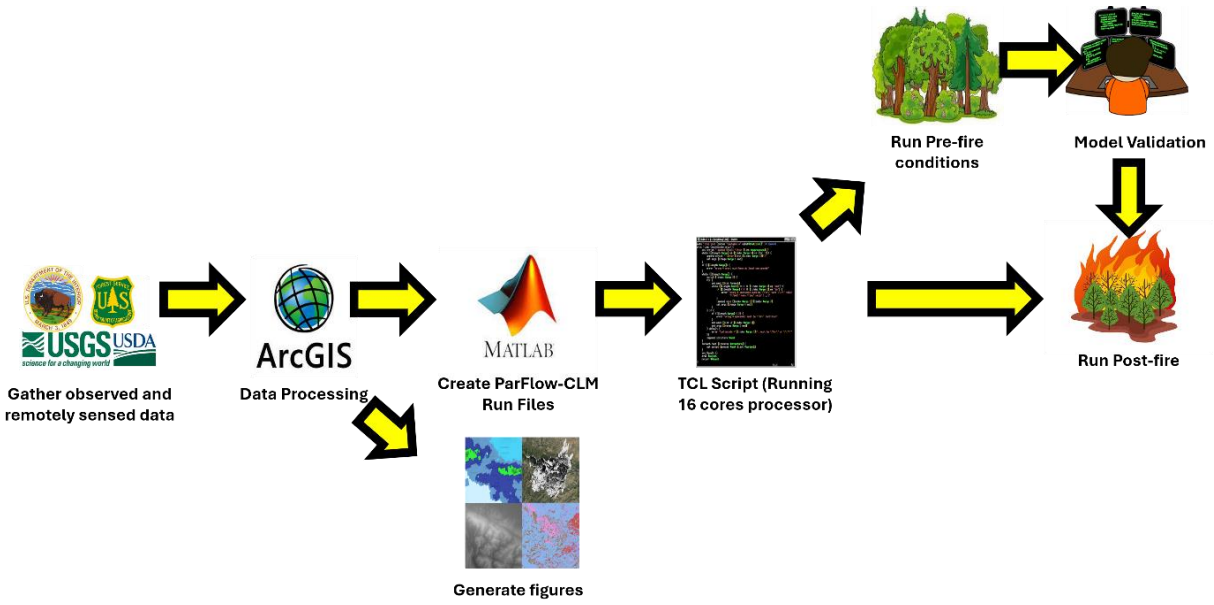


Figure 5: Project Workflow

After compiling the run files in MATLAB, the script initiates the model run within ParFlow-CLM. Utilizing a computer cluster, the research team had the flexibility to choose

the number of processors allocated for each run. For all the pre- and post-fire simulations, the team opted for 16 processing cores, distributing them with 4 in the x-direction, 4 in the y-direction, and 1 in the z-direction and running at an hourly timestep. Our post-processing script calculates surface storage, subsurface storage, surface runoff, evapotranspiration (2D), domain total evapotranspiration, transpiration, and soil evaporation.

Model Domain

The spin-up time can vary based on the selected model domain and time frame. On average, the spin-up time for all runs ranged from 100 to 121 restarts, with each run lasting 8 hours. This totals approximately 35 to 40 days of spin-up time. The time frame for the Delta fire is from September 05, 2016, to September 05, 2018, for pre-fire conditions. After completing this time frame, we follow up with post-fire conditions all the way through September 01, 2022. As for the Creek Fire, the pre-fire conditions are from September 04, 2018, to September 04, 2022. After completing this time frame for Creek Fire, we follow up with post-fire conditions all the way through September 01, 2022.

Our computational model for the Delta fire scenario encompasses a domain defined by 884 grid cells in the x-direction, 503 grid cells in the y-direction, and 15 grid cells in the z-direction, with grid spacings of 30 meters along the x and y axes, and 1 meter along the z-axis. The starting coordinates of the domain are 533385Northing and 4530362 Easting in UTM Coordinates. To compute the total space covered by the domain, we multiply the number of grid cells in each direction by their corresponding spacing: 26.52 kilometers in the x-direction, 15.1 kilometers in the y-direction, and 15 meters in the z-direction, resulting in a total domain space of approximately 6 km^3.

In ParFlow, the variable "dz" commonly signifies the vertical grid spacing or cell thickness within the computational domain's vertical direction for pre- and post-fire conditions. This parameter is essential for capturing the three-dimensional configuration of the subsurface environment, particularly in simulations involving groundwater flow, transport, and burned layer impact. The choice of vertical grid spacing is critical for achieving accuracy in representing the burn layer of the shallow portion of the surface. The topmost sections of the matrix generated by the MATLAB script are identified as the burn layers. The variable "nlayers" specifies the number of layers designated to model the depth of burn penetration. In the provided model example, four burn layers were employed, each having a thickness of 0.025 meters (or 2.5 cm).

Table 4: Variable discretization in the z-direction for the total depth (nx*dz = 884(Delta) and 1692(Creek))

Layer #	**Thickness (m)**
Depth 1	0.025
Depth 2	0.025
Depth 3	0.025
Depth 4	0.025
Depth 5	1.25
Depth 6	1.25
Depth 7	2.25
Depth 8	2.9
Depth 9	2.25
Depth 10	1.25
Depth 11	0.75
Depth 12	0.75
Depth 13	0.75
Depth 14	0.75
Depth 15	0.75

Model Validation

To verify the model's accuracy, we must compare our results to current Earth-observing satellites such as Moderate Resolution Imaging Spectroradiometer (MODIS). MODIS works based on remote sensing principles, capturing data by measuring the electromagnetic radiation reflected or emitted by the Earth's surface. It operates in thirty-six spectral bands and is designed to capture data in various spectral bands ranging from visible to infrared wavelengths. This instrument can collect information about Earth's surface and atmosphere, such as climate change, weather monitoring, and land cover mapping. (C.O Justice, J.R.G Townshend, E.F Vermote, E Masuoka, R.E Wolfe, N Saleous, D.P Roy, J.T Morisette, 2002) MODIS provides a high temporal resolution, capturing frequent images of the Earth's surface, essential for monitoring the dynamics of wildfire events. We utilized a product derived from MODIS called MOD16 to compare our ET parameters. The MOD16 product offers estimates of evapotranspiration (ET) at a spatial resolution of approximately 500 meters and a temporal resolution of 8 days, making it valuable for analyzing ET dynamics across various landscapes and over time. MOD16 focuses on providing estimates of actual evapotranspiration (ET) at a global scale. MOD16 algorithm employs a simplified form of the Penman-Monteith equation (Equation 6), a widely used method for estimating evapotranspiration. The equation considers land surface temperature, vegetation characteristics, and meteorological variables to calculate the amount of water vapor leaving the land surface due to evapotranspiration. (Yuan, Y. Ma, Chen, Wang, Li, 2021)

$$LE = \frac{\Delta*(R_{net}-G_0)+C_p*\rho_a*\frac{VPD}{r_a}}{\Delta+\gamma*(1+\frac{r_s}{r_a})} \quad \text{Eq 6}$$

Estimations of Evapotranspiration are essential for verifying the accuracy and stability of our model to ensure that the results being produced represent a high temporal resolution of what can occur as a result of a wildfire.

In our statistical analysis comparing ParFlow-CLM daily evapotranspiration simulations with observed data from ECOSTRESS and MODIS16, we utilized Pearson's Correlation (R). Pearson's correlation coefficient (Equation 7) measures the strength and direction of the linear relationship between two variables. It ranges from -1 to 1, where 1 indicates a perfect positive linear relationship, -1 indicates a perfect negative linear relationship, and 0 indicates no linear relationship. In our study, we compare the instantaneous daily ET from our modeling simulation to the total daily ET from both satellite products.

$$R = \frac{\Sigma_{i=1}^{N}\left((X_i-\overline{X})(Y_i-\overline{Y})\right)}{\sqrt{\Sigma_{i=1}^{N}(X_i-\overline{X})^2\ \Sigma_{i=1}^{N}(Y_i-\overline{Y})^2}} \quad \text{Eq 7}$$

Where X_i and Y_i are individual data points and $\overline{X}$ and $\overline{Y}$ are the means of the X and Y variables, respectively. We utilized scatter plots to depict the correlation and accuracy of the datasets, which offer a visual understanding of the overall pattern and distribution between the simulated and observed data. This approach involved comparing simulated versus observed ET products at shared daily observations, providing insights into how well the simulated data aligns with observed trends over time.

To properly compare our results with ECOSTRESS data, we applied a moving mean average function to the available data in MATLAB. Given that ECOSTRESS is relatively new, there are several data gaps within the timeframe of our study. By applying the moving mean average, we can effectively fill in these data gaps and enable a more robust comparison with the averaged values of existing data.

The use of a moving mean average helps to smooth out short-term fluctuations and highlight longer-term trends in the data, ensuring that our comparisons are more reliable. This approach not only allows us to address the issue of missing data but also enhances the overall quality of our analysis by reducing noise. Consequently, we can make more accurate and meaningful comparisons between our results and the ECOSTRESS data, thereby strengthening the validity of our findings.

CHAPTER 3

RESULTS

movIssues with Model Simulations

On May 1st, Dr. Lopez and I confirmed there was an issue accessing the Curie machine and messaged the administrators. They learned that the Head node on the Curie Cluster failed pausing all model simulations and preventing any users from accessing files on the cluster. It was down until May 6th, causing the loss of valuable computational time. As a result, I will be presenting only the results of the Delta Fire in the Results section for 09/05/2016 to 04/01/2019. It takes approximately 8 real-time hours to simulate 26 days for our large domain; we would have been able to complete an additional year in 4 days.

Observed vs Simulated

We conducted a comparative analysis of our simulated results with data from both ECOSTRESS and MODIS products, spanning from September 5, 2016, to April 01, 2019. While ECOSTRESS, introduced in 2018, provides valuable insights, its limited timeframe and sparse or unreliable observations restrict its dataset. Despite these limitations, ECOSTRESS managed to cover 09/01/2018 to 04/01/2019 of the observed data simulated in our studies. Conversely, with its more extended operational history, MODIS offers a broader temporal scope and more consistent observations.

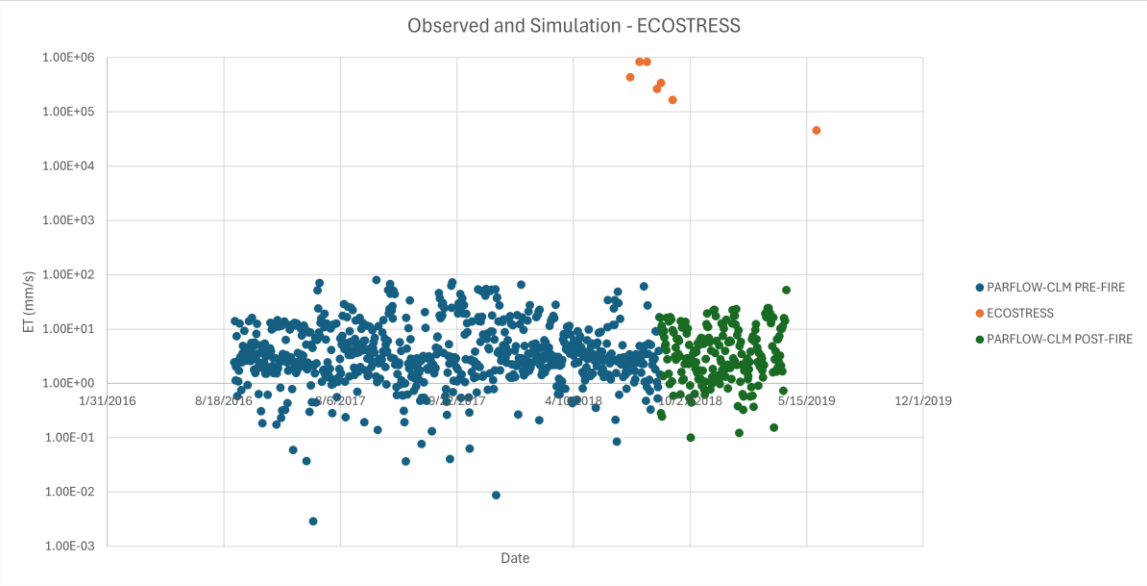


Figure 6: Raw ECOSTRESSV Data from 09/05/1/2018- 04/01/2019 Vs Pre/Post Fires Data for Slate Creek-Sacramento River, East Fork.

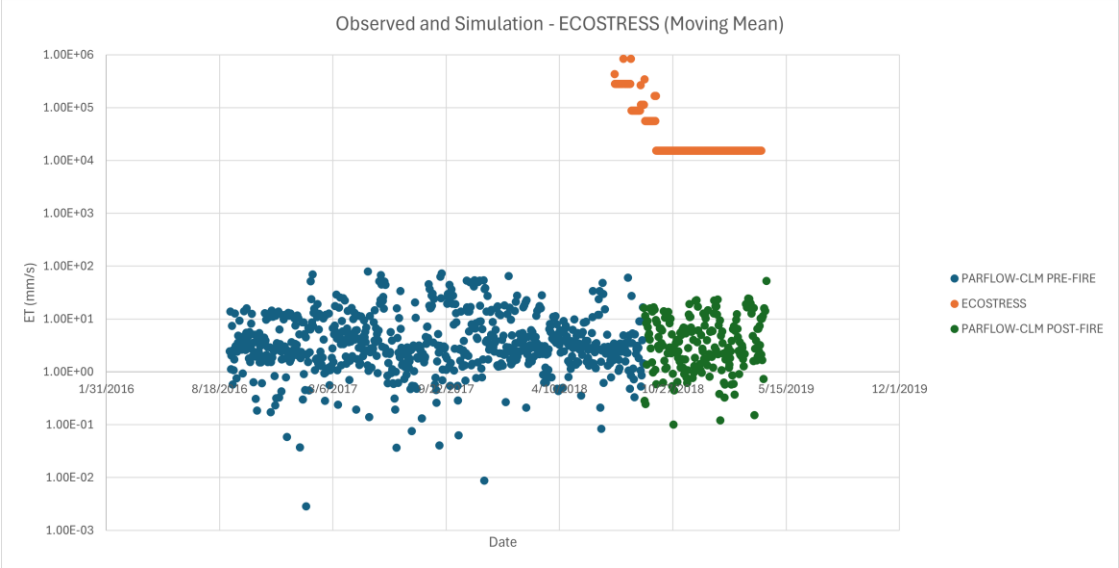


Figure 7: Moving Mean ECOSTRESSV Data from 09/05/1/2018- 04/01/2019 Vs Pre/Post Fires Data for Slate Creek-Sacramento River, East Fork

The graphs above illustrate the relationship between ECOSTRESS data, and our simulated Pre- and Post-Fire runs data. Although the ECOSTRESS dataset contains limited data for our current time frame, we can still observe a similar peak time among the three datasets. To further assist our observations, we plotted the moving mean average to fill in any missing data, better representing what ECOSTRESS could have provided. Simply comparing numeric results does not justify the accuracy of our model because the ECOSTRESS data represents a total sum of ET, whereas our model outputs instantaneous results. Due to this difference in data types, comparing the trends rather than the absolute values is more appropriate. Unfortunately, insufficient data was produced to compare the following dates after 04/01/2019 due to issues with the Curie Machine.

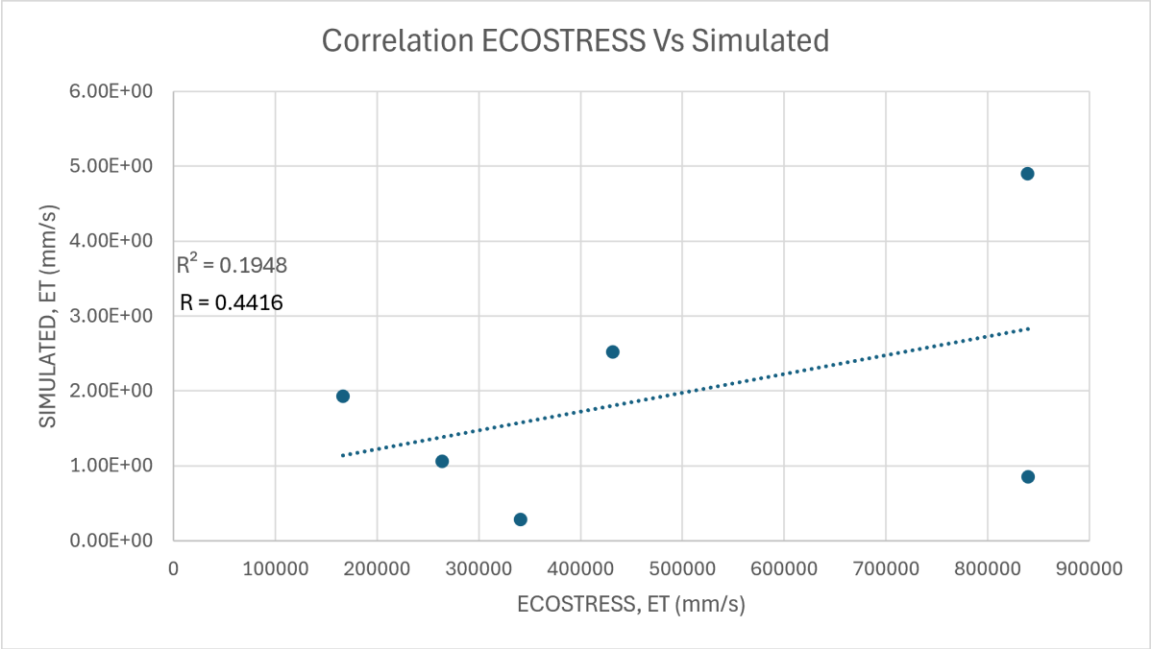


Figure 8: ECOSTRESS Vs. Simulated ET Correlation

The graph above illustrates the Correlation between ECOSTRESS and Pre-Post Fire Simulations. An R-value of 0.4416 indicates a moderate positive linear correlation between the two datasets. This means that, generally, as one dataset increases, the other dataset also increases, but the relationship is not very strong. While this value shows a positive trend, it is not close enough to 1 to be considered a strong correlation. It suggests that other factors or variabilities, such as the difference in data, influence the relationship between the datasets. In practical terms, this level of correlation implies that the simulated data has a moderate degree of accuracy in predicting or matching the observed data. There is a noticeable trend, but significant deviations from a perfect linear relationship are present.

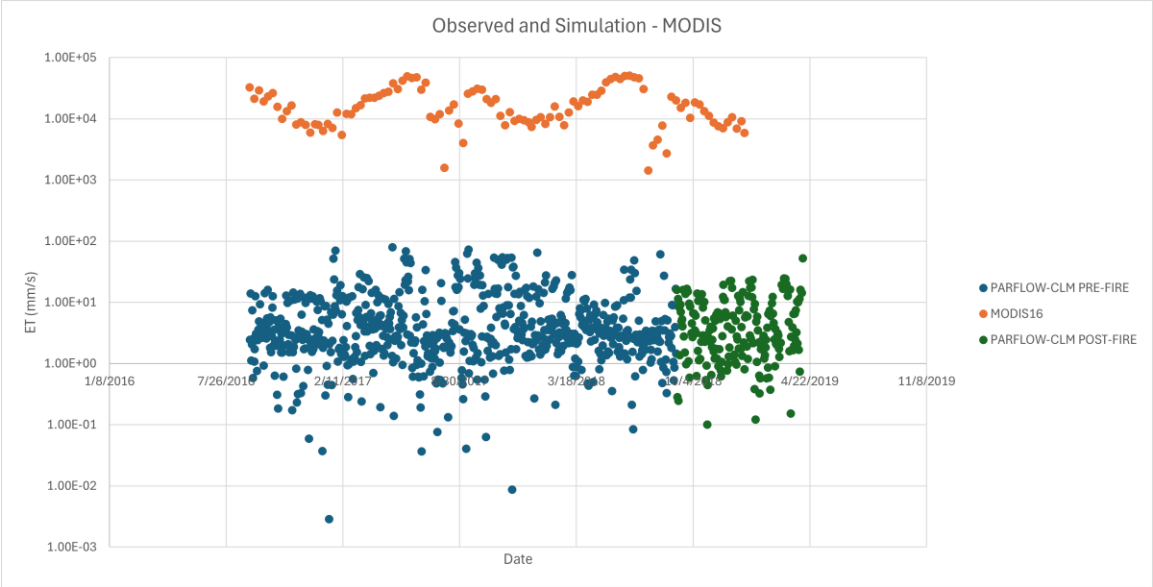


Figure 9: MODIS Data from 09/05/1/2016-04/01/2019 Vs Pre/Post Fires Data for Slate Creek-Sacramento River, East Fork.

The graphs above illustrate the relationship between MODIS data and our simulated Pre- and Post-Fire runs data. Unlike the ECOSTRESS dataset, the MODIS dataset provides a more extensive collection of data, allowing us to observe the peak trends between the simulated and observed data. The abundance of MODIS data enables a more robust comparison, highlighting the alignment of peak times across the datasets.

Again, we must emphasize that simply comparing numeric results does not fully justify the accuracy of our model because the MODIS data also represents the total sum of ET over the day, whereas our model outputs instantaneous results. This inherent difference in data types underscores the importance of comparing trends rather than absolute values. While the MODIS data shows similar peak times to our simulated data, there are also instances where the data diverges. These discrepancies can be at fault of several factors, including differences in spatial resolution and manual parameters inputs for ParFlow. Overall, the

detailed MODIS dataset plays a crucial role in validating our simulations and providing insights into the temporal patterns of ET before and after fire events.

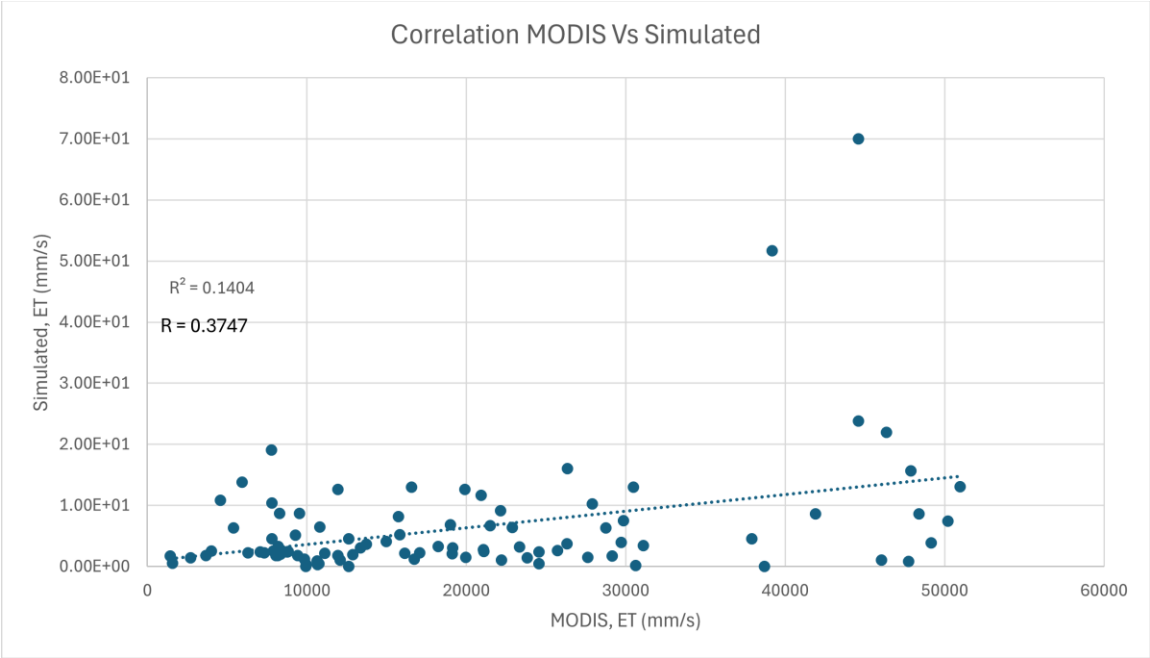


Figure 10: MODIS Vs. Simulated ET Correlation

In our analysis, the MODIS dataset provided a more extensive collection of data points, allowing for a more precise visualization of trends over time. The correlation between the MODIS weekly sums of Evapotranspiration (ET) and our simulated data yielded a Pearson's Correlation Coefficient (R) of 0.3747. This indicates a weak to moderate positive linear relationship. Despite the larger volume of data from MODIS, which spans weekly ET sums, the correlation coefficient of 0.3747 suggests that while there is a positive trend between the observed and simulated data, it is not particularly strong.

Data Limitations and Issues

One of the main challenges we encountered in our project was the scarcity of data from ECOSTRESS. As ECOSTRESS was launched in 2018 and began providing data from January

1 of that year, it wasn't until 2018 that we could conduct a more comprehensive comparison between ECOSTRESS and our simulations.

Configuring the model to operate effectively under fire conditions presented significant challenges, constituting a valuable learning experience for our team. Despite meticulous planning, the execution of the process encountered numerous unexpected hurdles, and the outcome diverged from our initial expectations. Over two months, during which the model remained inactive, we devoted considerable time and effort to troubleshooting and refining our approach, striving to ascertain the optimal settings and parameters necessary to achieve successful model operation under fire conditions. This downtime served as a critical period for experimentation and problem-solving, enabling us to gain insights and enhance our understanding of the complexities of simulating fire-related scenarios.

CHAPTER 4

CONCLUSION

In conclusion, our study faced significant challenges due to technical issues with the Curie machine, resulting in a loss of valuable computational time and limiting the scope of our analysis. Despite these setbacks, we successfully conducted a comparative analysis of our simulated results with data from ECOSTRESS and MODIS. ECOSTRESS provided limited insights into ET but was still valuable for ensuring the accuracy of our model. The extensive and consistent dataset from MODIS allowed for a more robust comparison, highlighting peak trends and validating our simulations.

Our findings indicate a moderate positive linear correlation between ECOSTRESS and our simulated data, with an R-value of 0.4416, and a weaker positive correlation with MODIS data, with an R-value of 0.3747, but offered more data to analyze. While not strong, these correlations suggest that our model can reasonably predict trends in evapotranspiration (ET) but also highlight significant deviations due to differences in data types, spatial resolution, and model parameters.

The primary limitation of our project was the restricted data availability from ECOSTRESS, which hindered a comprehensive comparison. Moreover, configuring the model to operate effectively under fire conditions posed significant challenges. Although unfortunate, the downtime due to the Curie machine failure provided an opportunity for extensive self-reflection and lessons learned that can influence better management of future studies.

REFERENCES

Stevens-Rumann, C. S., & Morgan, P. (2019). Tree regeneration following wildfires in the western US: a review. Fire Ecology, 15(1). https://doi.org/10.1186/s42408-019-0032-1

Zavala, L., De Celis, R., & Jordán, A. (n.d.). How wildfires affect soil properties. A brief review. Cuadernos De Investigación Geográfica, 40(2), 311–332. https://doi.org/10.18172/cig.2522

Pérez-Cabello, F., Montorio, R., & Alves, D. B. (2021). Remote sensing techniques to assess post-fire vegetation recovery. Current Opinion in Environmental Science & Health, 21, 100251. https://doi.org/10.1016/j.coesh.2021.100251

Ayala, J. J. H., Mann, J., & Grosvenor, E. (2021). Antecedent rainfall, excessive vegetation growth and its relation to wildfire burned areas in California. Earth and Space Science, 8(9). https://doi.org/10.1029/2020ea001624

Stevens-Rumann, C. S., & Morgan, P. (2019b). Tree regeneration following wildfires in the western US: a review. Fire Ecology, 15(1). https://doi.org/10.1186/s42408-019-0032-1

Jung, H. Y., Hogue, T. S., Rademacher, L. K., & Meixner, T. (2008). Impact of wildfire on source water contributions in Devil Creek, CA: evidence from end-member mixing analysis. Hydrological Processes, 23(2), 183–200. https://doi.org/10.1002/hyp.7132

Jensen, D., Reager, J. T., Zajic, B., Rousseau, N., Rodell, M., & Hinkley, E. (2018). The sensitivity of US wildfire occurrence to pre-season soil moisture conditions across ecosystems. Environmental Research Letters, 13(1), 014021. https://doi.org/10.1088/1748-9326/aa9853

Stavi, I. (2019). Wildfires in Grasslands and Shrublands: A review of impacts on vegetation, soil, hydrology, and geomorphology. Water, 11(5), 1042. https://doi.org/10.3390/w11051042

Miller, J. D., Skinner, C. N., Safford, H. D., Knapp, E. E., & Ramirez, C. M. (2012). Trends and causes of severity, size, and number of fires in northwestern California, USA. Ecological Applications, 22(1), 184–203. https://doi.org/10.1890/10-2108.1

Buhk, C., Meyn, A., & Jentsch, A. (2007). The challenge of plant regeneration after fire in the Mediterranean Basin: scientific gaps in our knowledge on plant strategies and evolution of traits. https://www.semanticscholar.org/paper/The-challenge-of-plant-regeneration-after-fire-in-Buhk-Meyn/a508ffb383e68976a7c4ae9be5efe7235d365c6a

Schnur, M. T., Xie, H., & Wang, X. (2010). Estimating root zone soil moisture at distant sites using MODIS NDVI and EVI in a semi-arid region of southwestern USA. Ecological Informatics, 5(5), 400–409. https://doi.org/10.1016/j.ecoinf.2010.05.001

Westerling, A. L., & Bryant, B. P. (2007). Climate change and wildfire in California. Climatic Change, 87(S1), 231–249. https://doi.org/10.1007/s10584-007-9363-z

Jones, M. W., Smith, A. J. P., Betts, R., Canadell, J. G., Prentice, I. C., Le Quéré, C., (2020). Climate change increases the risk of wildfires. In ScienceBrief Review [Journal-article]. https://sciencebrief.org/uploads/reviews/ScienceBrief_Review_WILDFIRES_Jan2020.pdf

Rodrigues, M., Ibarra, P., Echeverría, M., Pérez-Cabello, F., & De La Riva, J. (2014). A method for regional-scale assessment of vegetation recovery time after high-severity wildfires. Progress in Physical Geography, 38(5), 556–575. https://doi.org/10.1177/0309133314542956

Ebel, B. A., Moody, J. A., & Martin, D. A. (2012). Hydrologic conditions controlling runoff generation immediately after wildfire. Water Resources Research, 48(3). https://doi.org/10.1029/2011wr011470

Pradhan, N. R., & Floyd, I. (2021). Event based Post-Fire hydrological modeling of the Upper Arroyo Seco Watershed in Southern California. Water, 13(16), 2303. https://doi.org/10.3390/w13162303

Kinoshita, A. M., & Hogue, T. S. (2011). Increased dry season water yield in burned watersheds in Southern California. Environmental Research Letters, 10(1), 014003. https://doi.org/10.1088/1748-9326/10/1/014003

van Leeuwen, W.J.D. (2008) Monitoring the Effects of Forest Restoration Treatments on Post-Fire Vegetation Recovery with MODIS Multi-Temporal Data. Sensors, 8, 2017-2042. http://dx.doi.org/10.3390/s8032017

Stavi, I., Barkai, D., Knoll, Y. M., Glion, H. A., Katra, I., Brook, A., & Zaady, E. (2017). Fire impact on soil-water repellency and functioning of semi-arid croplands and rangelands: Implications for prescribed burnings and wildfires. Geomorphology, 280, 67–75. https://doi.org/10.1016/j.geomorph.2016.12.015

Clothier, B., Vogeler, I., & Magesan, G. (2000). The breakdown of water repellency and solute transport through a hydrophobic soil. Journal of Hydrology, 231–232, 255–264. https://doi.org/10.1016/s0022-1694(00)00199-2

DeBano, L. (2000). The role of fire and soil heating on water repellency in wildland environments: a review. Journal of Hydrology, 231–232, 195–206. https://doi.org/10.1016/s0022-1694(00)00194-3

Cawson, J. G., Nyman, P., Smith, H. G., Lane, P. N., & Sheridan, G. J. (2016). How soil temperatures during prescribed burning affect soil water repellency, infiltration and erosion. Geoderma, 278, 12–22. https://doi.org/10.1016/j.geoderma.2016.05.002

Stisen, S., Jensen, K. H., Sandholt, I., & Grimes, D. I. (2008). A remote sensing driven distributed hydrological model of the Senegal River basin. Journal of Hydrology, 354(1–4), 131–148. https://doi.org/10.1016/j.jhydrol.2008.03.006

Kittel, C. M. M., Nielsen, K., Tøttrup, C., & Bauer-Gottwein, P. (2018). Informing a hydrological model of the Ogooué with multi-mission remote sensing data. Hydrology and Earth System Sciences, 22(2), 1453–1472. https://doi.org/10.5194/hess-22-1453-2018

Kollet, S. J., & Maxwell, R. M. (2008). Capturing the influence of groundwater dynamics on land surface processes using an integrated, distributed watershed model. Water Resources Research, 44(2). https://doi.org/10.1029/2007wr006004

Maxwell, R. M., Condon, L. E., & Kollet, S. (2015). A high-resolution simulation of groundwater and surface water over most of the continental US with the integrated hydrologic model ParFlow v3. Geoscientific Model Development, 8(3), 923–937. https://doi.org/10.5194/gmd-8-923-2015

Atchley, A. L., Kinoshita, A. M., Lopez, S. R., Trader, L., & Middleton, R. (2018). Simulating surface and subsurface water balance changes due to burn severity. Vadose Zone Journal, 17(1), 1–13. https://doi.org/10.2136/vzj2018.05.0099

Fisher, J. B., Lee, B., Purdy, A. J., Halverson, G. H., Dohlen, M. B., Cawse-Nicholson, K., Wang, A., Anderson, R. G., Aragon, B., Arain, M. A., Baldocchi, D. D., Baker, J. M., Barral, H., Bernacchi, C. J., Bernhofer, C., Biraud, S. C., Bohrer, G., Brunsell, N., Cappelaere, B., . . . Hook, S. (2020). ECOSTRESS: NASA's next generation mission to measure evapotranspiration from the International Space Station. Water Resources Research, 56(4). https://doi.org/10.1029/2019wr026058

Meerdink, S. K., Hook, S. J., Roberts, D. A., & Abbott, E. A. (2019). The ECOSTRESS spectral library version 1.0. Remote Sensing of Environment, 230, 111196. https://doi.org/10.1016/j.rse.2019.05.015

Wang, Y., Li, Z., Feng, Q., Si, L., Gui, J., Cui, Q., Zhao, Y., & Xu, C. (2024). Global evapotranspiration from high-elevation mountains has decreased significantly at a

rate of 3.923 %/a over the last 22 years. Science of the Total Environment, 172804. https://doi.org/10.1016/j.scitotenv.2024.172804